

Information scrambling and entanglement in quantum approximate optimization algorithm circuits

Chen Qian,^{1,2,*} Wei-Feng Zhuang,¹ Rui-Cheng Guo,² Meng-Jun Hu,¹ and Dong E. Liu^{1,2,3,†}

¹*Beijing Academy of Quantum Information Sciences, Beijing 100193, China*

²*State Key Laboratory of Low Dimensional Quantum Physics,
Department of Physics, Tsinghua University, Beijing, 100084, China*

³*Frontier Science Center for Quantum Information, Beijing 100184, China*

Variational quantum algorithms, which consist of optimal parameterized quantum circuits, are promising for demonstrating quantum advantages in the noisy intermediate-scale quantum (NISQ) era. Apart from classical computational resources, different kinds of quantum resources have their contributions in the process of computing, such as information scrambling and entanglement. Characterizing the relation between complexity of specific problems and quantum resources consumed by solving these problems is helpful for us to understand the structure of VQAs in the context of quantum information processing. In this work, we focus on the quantum approximate optimization algorithm (QAOA), which aims to solve combinatorial optimization problems. We study information scrambling and entanglement in QAOA circuits respectively, and discover that for a harder problem, more quantum resource is required for the QAOA circuit to obtain the solution in most of the cases. We note that in the future, our results can be used to benchmark complexity of quantum many-body problems by information scrambling or entanglement accumulation in the computing process.

I. INTRODUCTION

Quantum computation is considered to have a crucial computational speed-up compared with classical computing, because it consumes not only classical computational resources but also quantum resources [1]. As the most important feature of quantum mechanics, entanglement offers essential resource for quantum computation [2, 3]. Besides, since quantum circuits are actually unitary channels, the quantity characterizing spatiotemporal entanglement properties of a channel, namely information scrambling, should be viewed as a considerable resource as well [4–8]. The concept of information scrambling was first introduced by Hayden and Preskill [9] to demonstrate that the quantum information of a diary thrown into a black hole will spread to the whole system, and finally recover from the black hole evaporation. In last decades, studies of this physical process mostly focus on the area of black hole information and quantum gravity [10, 11]. Currently, it has been demonstrated that for the H-P protocol, scrambled information can be efficiently decoded using a Clifford decoder, provided that the system is not fully chaotic [12, 13]. Recently, more and more works turn their attention to information scrambling in quantum circuits, which pave the way to applications involving benchmarking noise [14], recovering lost information [15], characterizing performance of quantum neural networks [16–18], unifying chaos and random circuits [19, 20], and so on [21, 22]. In addition, the process of information scrambling is observed experimentally on superconducting quantum processors [23, 24]. Briefly, studying information scrambling

and entanglement properties offers us an overview of how much quantum resource is needed for specific quantum circuits.

Variational quantum algorithms (VQAs) belong to the leading strategies to potentially present quantum advantage on near-term NISQ devices [5], which include a series of algorithms such as variational quantum eigensolver (VQE) [25], quantum machine learning (QML) [26] and quantum approximate optimization algorithm (QAOA) [27]. VQAs share the common structure of optimizing parameters with a classical optimizer and running parameterized quantum circuits to solve problems. In particular, QAOA is proposed to solve the quadratic unconstrained binary optimization (QUBO) problems [28], which can be translated into computing minimal expectation values of an Ising Hamiltonian. Based on these settings, QAOA is widely applied in combinatorial optimization problems, e.g., traffic congestion, finance, and many-body physics [29, 30]. It is useful to give a thorough analysis to the scrambling and entanglement properties of the optimal parameterized quantum circuits in order to benchmark the quantum resource consumed when we utilize VQAs to calculate a certain problem.

The role of entanglement for VQAs has been extensively studied from different perspectives [31–35]. In recent papers, bipartite entanglement entropy in p -layer QAOA circuits was investigated. Chen, *et al.* compared the entanglement required between ADAPT-QAOA and standard QAOA solving certain problems [33], and Dupont, *et al.* characterize entanglement generated in QAOA circuit with entanglement volume law [34]. However, details about entanglement generation in the p -layer circuit and its connection to complexity of problems still remains an open question. Moreover, in the aspect of information scrambling, Shen, *et al.* established a corre-

* qianchen@baqis.ac.cn

† dongeliu@mail.tsinghua.edu.cn

lation between scrambling ability and loss function in the training process of quantum neural networks [16], which raises an interesting question of whether a comparable correlation occurs in QAOA.

Therefore, our aim in this paper is to investigate the connection between complexity of QUBO problems and quantum resource (including information scrambling and entanglement) consumed in the QAOA circuits. In this work, we address a special type of QUBO problems whose solutions are non-degenerate in order to concentrate on the quantum resource generated during the computing process. When we embed these solutions to quantum circuits, the target states are product states. Since both initial and final states have no entanglement, all quantum resource generated in the circuit is only for computing steps. As we have fixed all basic settings of the optimization algorithm, we can build a clear link between the amount of quantum resources used in QAOA circuits and the complexity to solve QUBO problems.

Next, we need to discriminate the concept “complexity of QUBO problems”. This concept includes two different definitions [28]:

1. The complexity to solve a QUBO problem mathematically, which is highly dependent on structure of the graph.

2. The computational difficulty of solving a QUBO problem using certain algorithms. Both algorithm and properties of the graph are relevant to this computational complexity.

The two complexities may not have a definitive correlation. As we have discussed, the mathematical complexity of a QUBO problem depends on its geometric structure, such as edges and weights. Usually, a mathematically harder problem is more difficult to solve using algorithms on a classical or quantum computer as well. However, for different algorithms, the difficulty to solve these QUBO problems may be different. In this work, we only discuss solving QUBO problems via QAOA, thus we take the second definition to “complexity of QUBO problems” throughout this paper. Although a general mathematical expression of computational complexity of solving QUBO problems via QAOA is still an open question, at least it is determined by some important attributes of a QUBO graph, like

$$\mathcal{C} \sim f(D, w_{ij}, h_k), \quad (1)$$

where D is the density of a graph, w_{ij} and h_k are weights of edges and nodes of the graph, detailed definitions are introduced in Sec. II A.

Based on all above settings, we present our results in two parts: Firstly, we treat the QAOA circuit as a quantum channel to compare information scrambling characterized by tripartite information with QAOA computational complexity characterized by success rates, and our results are obtained for three different kinds of QUBO problems. Secondly, we compare entanglement accumulation in QAOA circuit with five QUBO problems where the corresponding graphs have different edges but the

weights of edges and nodes are the same. Notably, we propose a quantity to characterize entanglement accumulation inside QAOA circuit, which has the form of average area of entanglement entropy generated during the evolution of the quantum circuit. Finally, we claim that for every cases we consider, at least for shallow circuits, there exists a positive correlation between the complexity of QUBO problems and information scrambling, as well as between the complexity and entanglement.

In what follows, we first briefly review the background of QAOA and tripartite information and introduce our implementation in Sec. II, and then compare information scrambling and entanglement entropy with complexity of problems in Sec. III and Sec. IV respectively. At last, we discuss our results and provide future lines of research in Sec. V.

II. PRELIMINARIES

In this section, we briefly review the basic concepts on QAOA and tripartite mutual information describing information scrambling. After that, we introduce our basic settings in this work.

A. The quantum approximate optimization algorithm

As we discussed in Sec. I, QAOA is a quantum algorithm aiming to solve combinatorial optimization problems, which was first brought by Farhi, *et al.* [27]. Usually, a combinatorial optimization problem can be represented by a QUBO model, where we can associate a weighted graph $G = (V, E)$ with nodes $V = \{1, 2, \dots, N\}$ and edges $E = \{(i, j), i \neq j\}$. In this graph, the weight of the edge $\{i, j\}$ is denoted by w_{ij} , and the weight of the node k is denoted by h_k . Connection property of the graph can be characterized by density of the graph:

$$D = \frac{2E}{N(N-1)}, \quad (2)$$

where E is the number of edges and $N(N-1)/2$ is the maximal potential connections. The graph can be mapped into an Ising model in quantum many-body physics with V represents independent terms Z_i and E represents interaction terms $Z_i Z_j$. Therefore, the most general form of an Ising Hamiltonian reads

$$H_C = \sum_{i,j=1}^N w_{ij} Z_i Z_j + \sum_{k=1}^N h_k Z_k, \quad (3)$$

where Z_i are σ_z operators with eigenvalues ± 1 , w_{ij} and h_k are coupling strengths of the interaction and independent terms. The target of QAOA is to achieve the minimal quantum mean value $\langle H_C \rangle$ via optimized parameters. Here, the QAOA circuit with p -layer and $2p$

parameters is as follows

$$|\vec{\beta}, \vec{\gamma}\rangle = U_B(\beta_p) U_C(\gamma_p) \cdots U_B(\beta_1) U_C(\gamma_1) \mathbf{H}^{\otimes N} |0\rangle^{\otimes N}, \quad (4)$$

where $U_B(\beta_i) = e^{-i\beta_i H_B}$, $H_B = \sum_{i=1}^N X_i$, $U_C(\gamma_i) = e^{-i\gamma_i H_C}$, and \mathbf{H} means Hardward gate. The $2p$ parameters $\vec{\beta} = (\beta_1, \beta_2, \cdots, \beta_p)$ and $\vec{\gamma} = (\gamma_1, \gamma_2, \cdots, \gamma_p)$ are optimized by classical optimization algorithm, after that they are applied to the parameterized quantum circuit Eq. (4) to obtain a smaller mean value $\langle H_C \rangle$. When QAOA finds the minimum of $\langle H_C \rangle$, it outputs a set of optimal parameters $\{\vec{\beta}_{opt}, \vec{\gamma}_{opt}\}$ at the same time, here state $|\vec{\beta}_{opt}, \vec{\gamma}_{opt}\rangle$ is the ground state of Eq. (3).

We note that $\{\vec{\beta}_{opt}, \vec{\gamma}_{opt}\}$ has multiple solutions for a certain H_C as one choose different initial parameters $\{\vec{\beta}_0, \vec{\gamma}_0\}$. The choice of $\{\vec{\beta}_0, \vec{\gamma}_0\}$ may result in seeking $\{\vec{\beta}_{opt}, \vec{\gamma}_{opt}\}$ of the problem easier or harder. Thus, to characterize properties of QAOA circuits solving the problem H_C with less bias, we should turn to statistical average values of numerous samplings with random initial parameters.

B. Information scrambling and entanglement

The ‘‘butterfly effect’’ in quantum systems, where localized quantum information spreads to degrees of freedom of the entire system as a result of a small disturbance, is referred to as information scrambling. Hosur, *et al.* use information scrambling to characterize the ability of a channel to process quantum information, they quantify scrambling as tripartite mutual information, which can be understood as entanglement between input and output of the channel [4]. For any unitary channel \hat{U} in a N -qubit Hilbert space, it can be decomposed to

$$\hat{U} = \sum_{i,j=1}^{2^N} U_{ij} |i\rangle \langle j|, \quad (5)$$

where $\{|i\rangle\}$ is the basis of 2^N Hilbert space. Denoting $\{|i\rangle\}$ as the basis of N -qubit input legs and $\{|j\rangle\}$ as the basis of N -qubit output legs, the unitary operator \hat{U} can be mapped to a state $|U\rangle$ in the form of

$$|U\rangle = \sum_{i,j=1}^{2^N} \frac{U_{ij}}{\sqrt{2^n}} |i\rangle |j\rangle, \quad (6)$$

which represents an entanglement state of input qubits and output qubits. Since $|U\rangle$ is a pure entangled state, we can define entanglement entropy between input and output states. Usually we divide the input part into subsystems A and B , and output part into C and D , then entanglement entropy of AC reads

$$S_{AC} = -\text{Tr}(\rho_{AC} \log_2 \rho_{AC}), \quad (7)$$

where $\rho_{AC} = \text{Tr}_{BD}(|U\rangle \langle U|)$. Similarly, mutual information between A and C can be obtained as

$$I(A : C) = S_A + S_C - S_{AC}, \quad (8)$$

which can be understood as how much information from input subsystem A spread into output subsystem C via the channel \hat{U} . Considering different conditions the information spreading from A to C and D , tripartite mutual information is introduced with the form

$$I_3(A : C : D) = I(A : C) + I(A : D) - I(A : CD), \quad (9)$$

which is well-defined to characterize information scrambling. If there is no scrambling, all information of A will be found in C or D (suppose $|A| < |C|, |D|$), either $I(A : C)$ or $I(A : D)$ equals to $I(A : CD)$ and another one equals to zero, then Eq. (9) turns to be zero. If information of A is fully scrambled to the whole output system, we cannot recover the information only by accessing C or D , which means $I(A : C) = I(A : D) \sim 0$, then we obtain $I_3(A : C : D) \sim -I(A : CD) \sim -2|A|$.

Tripartite mutual information is also defined as topological entanglement entropy in topological quantum field theory [36], which is topologically invariant and represents a universal characterization of the many-body entanglement in the ground state of a topologically ordered two-dimensional system.

C. Implementation

Here we introduce some settings throughout the paper. For QAOA circuit, we use the package of *Qcover* to perform our simulations [37], the classical optimization algorithm we choose is Constrained Optimization BY Linear Approximation (COBYLA). The number of qubits of problems we consider is all $N = 7$.

By taking the QAOA circuits as unitary channels to study information scrambling, we build up subsystems of $A(|A| = 1)$, $B(|B| = 6)$, $C(|C| = 3)$ and $D(|D| = 4)$ in Fig. 1. Denoting that there are 245 combinations for $ABCD$ with the same number of qubits, since QAOA circuits have no natural choice of these subsystems. We have tried several other combinations and find even $I_3(A : C : D)$ are different in values, the tendency in our results is invariant. Because tripartite information is a universal quantity describing scrambling ability of a channel, one choice is enough to reflect properties of the circuit we work on.

To study entanglement properties in detail, we consider von Neumann entanglement entropy of one qubit in the QAOA circuit. Since entanglement entropy of one random qubit cannot imply the full structure of the entanglement properties, we compute average values of Von-Neumann entropy for every qubits in the form of

$$\bar{S} = \frac{-\sum_{i=1}^N \text{Tr}(\rho_i \log_2 \rho_i)}{N}, \quad (10)$$

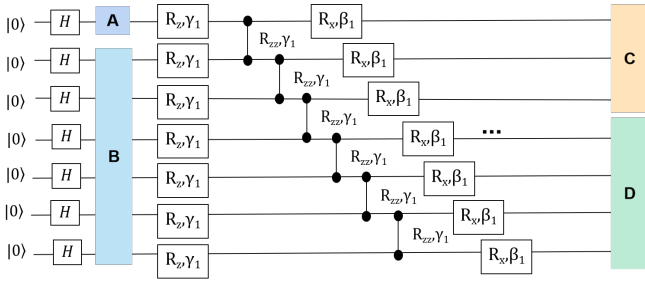


FIG. 1. One layer of QAOA circuit and our choice of subsystems $ABCD$.

where $\rho_i = \text{Tr}_{-i} \left(\left| \vec{\beta}_{opt}, \vec{\gamma}_{opt} \right\rangle \left\langle \vec{\beta}_{opt}, \vec{\gamma}_{opt} \right| \right)$ is the reduced density matrix after tracing out information of all qubits except the i th qubit from final state computed by QAOA.

Finally, we come to a concrete definition of complexity of QUBO problems. We have introduced the attributes relevant to complexity in Eq. (1) according to Ref. [28], and now we need a corresponding function deduced from QAOA computing results to reflect this complexity. For a certain computing result $\left| \vec{\beta}_{opt}, \vec{\gamma}_{opt} \right\rangle$, we take the distance between quantum mean value $\langle H_C \rangle$ and exact solution of the problem E_C to be [38, 39]

$$\alpha = \frac{\langle H_C \rangle}{E_C}. \quad (11)$$

The value was first introduced to benchmark the accuracy of approximate optimization algorithms [40, 41]. As the initial parameters of QAOA are chosen randomly, if we compute the same problem for different times, the final parameters can be distinct from each other, which lead to different α values. We can only say, a harder problem has less probability for QAOA to achieve a high α value. Thus, in this work we characterize complexity of a QUBO problem as a statistical probability when the α value is larger than a certain bound we expect in a number of samplings. That is, if we sample a QUBO problem n times and among them there are s samples whose α values larger than the bound we set, then the complexity of the problem is a rate

$$R = \frac{s}{n}, \quad (12)$$

which is also named as “success rate” [32]. In ideal circumstances, this rate should be negatively correlated with complexity \mathcal{C} as

$$\mathcal{C} \propto \frac{1}{R}. \quad (13)$$

However, some problems, such as local minima problem caused by gradient based optimization algorithm [42], in QAOA may suppress R and break the relation, which will be discussed in Sec. III.

III. SCRAMBLING IN QAOA CIRCUIT VERSUS COMPLEXITY OF THE PROBLEMS

In this section, we investigate quantum information scrambling in QAOA circuits. The circuits are designed specially for solving QUBO problems with non-degenerate solutions, whose corresponding Ising Hamiltonians H_C have separable ground states. As we have introduced in Sec. II B, we take the circuits as unitary channels and quantify scrambling ability of the channels by tripartite information I_3 . Our aim is to find some correlation between complexity of the problems and tripartite information.

A. Comparison between different kinds of graphs

As a start of this subsection, we first go back to the function of complexity Eq. (1). As we have fixed the degeneracy of QUBO solutions and basic settings of QAOA, the computational complexity of QUBO problems should only relate to two factors: density of the graph D and weights of the graph $\{w_{ij}, h_k\}$. In order to present a clear comparison, in the following we choose three typical kinds of graphs:

1. Linear graphs with their corresponding Ising Hamiltonians in the form of $Z - ZZ$.
2. Complete graphs with their corresponding Ising Hamiltonians in the form of $Z - ZZ$.
3. Linear graphs with their corresponding Ising Hamiltonians in the form of $Z + ZZ$.

Among the three cases, the 1st and 2nd cases have fixed graph weights but differ in graph density, whereas the 1st and 3rd cases have fixed graph density but differ in weights. According to Eq. (13), we expect if we fix one factor and change the other, the success rate R will evolve monotonically.

1. *Linear graph with $Z - ZZ$ -type Hamiltonian:* This kind of Ising Hamiltonians have only neighborhood interactions, which have the form of

$$H_{linear} = +w \sum_{i=1}^N Z_i - \sum_{i=1}^{N-1} Z_i Z_{i+1}, \quad (14)$$

where w is a weight parameter with $w \in [0.5, 1.5]$. Since all QUBO problems corresponding to this kind of graphs have non-degenerate solutions, their Ising Hamiltonians share the same ground states $|1\rangle^{\otimes N}$. As is shown in Fig. 2(a), success rate R increases as the number of layers in QAOA circuit increases, and then becomes saturated after $p \sim 6$. From Fig. 2(b) we note that even I_3 is very small, the positive correlation between $|I_3|$ and success rate is still visible.

To quantify the correlation, we introduce Pearson correlation coefficient here. Generally, Given two data sets X and Y , the correlation between them can be charac-

terized by

$$\rho_{XY} = \frac{\sigma_{XY}}{\sigma_X \sigma_Y}, \quad (15)$$

where σ_{XY} is their covariance, σ_X and σ_Y are their own variances. If two data sets have positive correlation, Pearson correlation coefficient takes the range of $(0, 1]$. Now, by taking the data of $|I_3|$ and R in Fig. 2(b), we can obtain the Pearson correlation coefficient $\rho_{I_3 R} \approx 0.4297$, which indicates an obvious positive correlation.

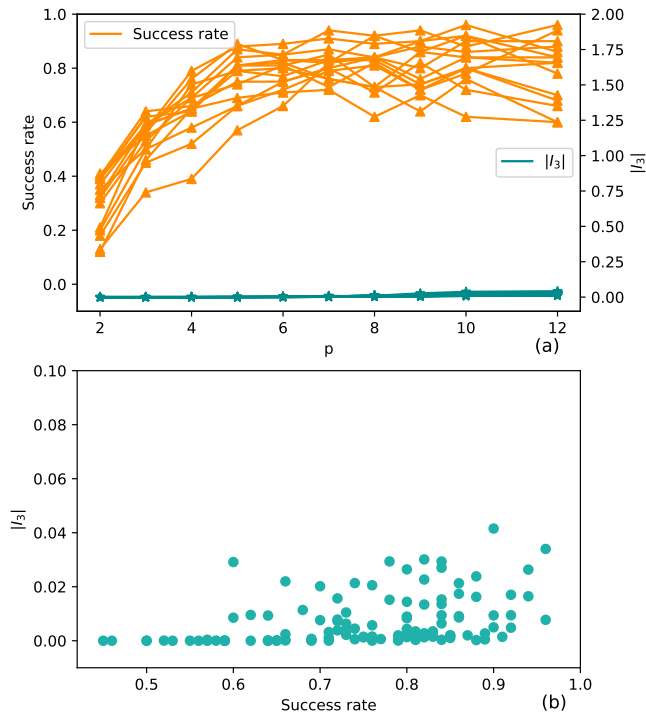


FIG. 2. The comparison between success rates to solve $\langle H_{linear} \rangle_{min}$ and information scrambling in the circuits with number of qubits $N = 7$ for the *linear* model of $Z - ZZ$ -type Hamiltonians. Here $w \in [0.5, 1.5]$, we randomly choose 15 different weights. (a). In this figure, each point represents a p -layer QAOA circuit to compute $\langle H_{linear} \rangle_{min}$ with one randomly chosen w . We loop the QAOA circuit 10^2 times, use Eq. (12) to obtain a success rate (orange point), and take an average value of I_3 (dark green point). We keep using these settings in all following $R - p$ and $I_3 - p$ figures. The orange lines are success rates of QAOA with different layers, where we set $\alpha \geq 0.996$, and entanglement entropy of C and D in final state ≤ 0.02 . There are 15 lines in the figure, representing 15 problems solved by QAOA with different weights w . The dark green lines are average values of $|I_3|$ in these QAOA circuits corresponding to the orange lines. (b). Using the data from (a), we show a correlation plot for R and $|I_3|$ from the same circuit (same p and w).

2. *Complete graph with $Z - ZZ$ -type Hamiltonian:* For complete graphs, the corresponding Ising Hamiltonians

are

$$H_{complete} = +w \sum_{i=1}^N Z_i - \sum_{i,j=1, i \neq j}^N Z_i Z_j, \quad (16)$$

where $w \in [0.5, 1.5]$ and each pair of nodes is connected by an edge. See Fig. 3(a) we can find that, looking for the minimal mean value of Eq. (16) is much harder than Eq. (14), since the success rates are much lower compared with the linear case especially for small layers. In this case, Eq. (16) have the same range of weights as Eq. (14), but the graph density is much larger than Eq. (14). It seems when we fix the weights, more connections make the QUBO problems harder to solve. About this issue, more details will be discussed in the next subsection. The success rates grow fast after $p \sim 8$, tripartite information also grows to about -1.86 simultaneously. From Sec. II B we have known the maximal tripartite information $I_3(A : C : D)$ is $-|A| \sim -2$, this means information encoded in the initial state $|+\rangle^{\otimes N}$ should be sufficiently scrambled to reach the exact final state $|1\rangle^{\otimes N}$ in the computing process.

Moreover, a positive correlation is also presented in Fig. 3(b). Using Eq. (15) we know Pearson correlation coefficient in this case is $\rho_{I_3 R} \approx 0.6581$. The correlation between tripartite information I_3 and success rate R seems stronger than the above linear graph case. This phenomenon can be observed in Fig. 2 and Fig. 3, as the layer p goes on, R stops increasing at some value in Fig. 2(a) whereas R in Fig. 3(a) keeps increasing. Ideally, in a QAOA circuit, more layers indicate a more optimal result, and therefore a larger R value. However, the classical optimization algorithm of QAOA is gradient based, when the function is complex and has many parameters, the minima evaluated by gradients may be far from the global minimum [42]. This problem is an obstacle of all VQAs. For QAOA, more layers bring a larger optimal parameter space, which may leads to more local minima and suppress the value of R .

3. *Linear graph with $Z + ZZ$ -type Hamiltonian:* Now we study linear graphs with very different weights from Eq. (14), namely

$$H'_{linear} = + \sum_{i=1}^N Z_i + v \sum_{i,i+1}^{N-1} Z_i Z_{i+1}, \quad (17)$$

where $v \in [2, 3]$ is the weight of edges ZZ . Unlike above cases, it is not easy to find the ground state at first glance. Among all 128 basis of the 7-qubit system, we find the product state $|1010101\rangle$ makes Eq. (17) take the minimal mean value.

As is shown in Fig. 4, success rate (we set $\alpha > 0.96$) are ~ 0 before $p = 15$, even when $p > 15$ the probabilities are much smaller than above cases. Compared with Fig. 2, it is much harder to obtain a good result of ground state

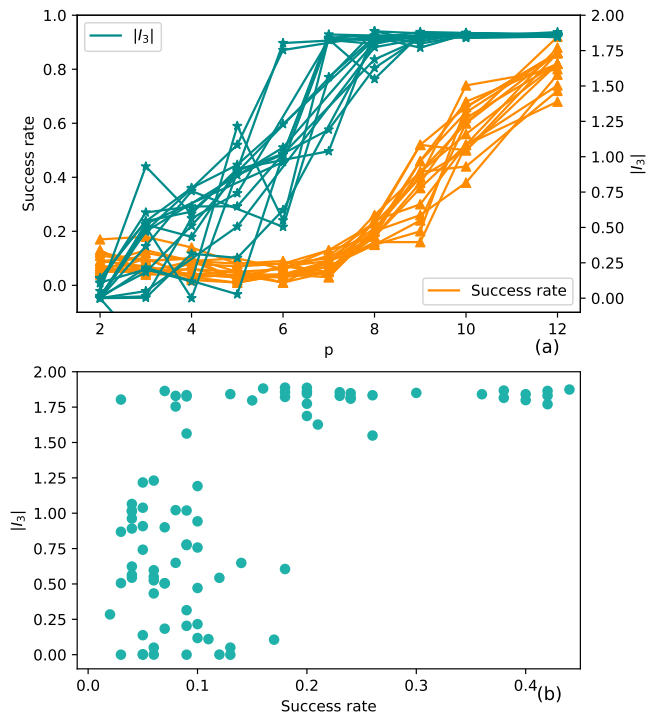


FIG. 3. The comparison between success rates for p -layer QAOA to compute $\langle H_{complete} \rangle_{min}$ and information scrambling in the circuit for different layers with number of qubits $N = 7$ for the *complete* model with $Z - ZZ$ -type Hamiltonians. Here $w \in [0.5, 1.5]$, we randomly choose 15 w s, and we take 10^2 loops as well. (a). The orange lines are success rates of QAOA of different layers to compute $\langle H_{complete} \rangle_{min}$ with different w s, with the condition $\alpha \geq 0.996$, and entanglement entropy of C and D in final state ≤ 0.02 . The dark green lines are $|I_3|$ in these QAOA circuits corresponding to the orange lines. (b). Using the data from (a), we show a correlation plot for R and $|I_3|$ from the same circuit.

energy, and it seems more tripartite information is generated in the circuit. We note that, density of the graph D of Eq. (17) is the same as Eq. (14), however different weights seem have a large contribution to complexity of the problems. With D fixed, we propose the complexity C can be expressed as

$$C \propto g(w_{ij}, h_k), \quad (18)$$

where $g(w_{ij}, h_k)$ only depends on weights of the graph. For the correlation between success rate and information scrambling, we get the Pearson correlation coefficient between tripartite information and success rate of Eq. (17) is $\rho_{I_3 R} \approx 0.4461$. The correlation strength is similar to the first linear graph case.

Having presented the positive correlation between tripartite information I_3 and success rate R in the above three cases, let us estimate a possible relation between the two variables. As we have noticed, both I_3 and R have upper bounds, and both of them increase fast at beginning then slow down when p becomes larger. Therefore, we can try to fit the data presented in Fig. 2-4 via

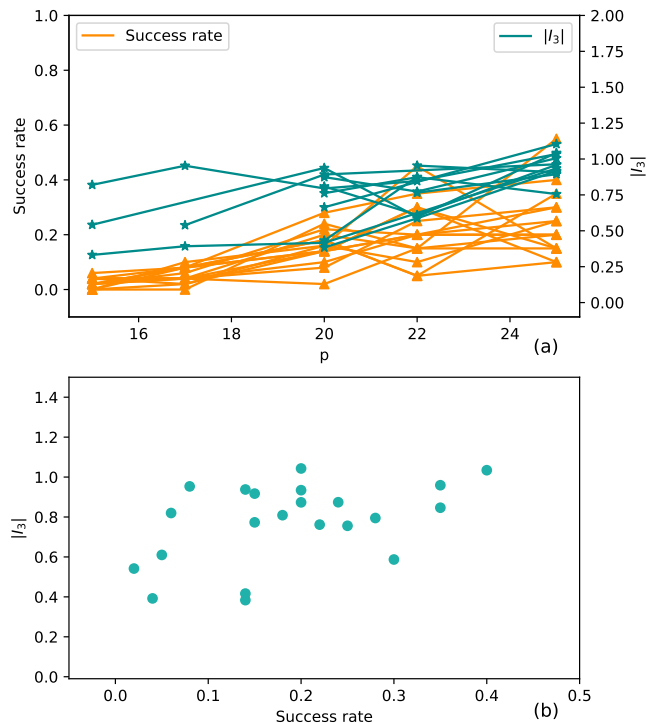


FIG. 4. The comparison between success rates for p -layer QAOA to compute $\langle H'_{linear} \rangle_{min}$ and information scrambling in the circuit for different layers with number of qubits $N = 7$ for the *linear* model with $Z + ZZ$ -type Hamiltonians. Here $v \in [2, 3]$, we randomly choose 15 v s, and we take 10^2 loops as well. (a). The orange lines are success rates of QAOA of different layers to compute $\langle H'_{linear} \rangle_{min}$ with different v s, with the condition $\alpha \geq 0.96$, and entanglement entropy of C and D in final state ≤ 0.25 . The dark green lines are $|I_3|$ in these QAOA circuits corresponding to the orange lines. (b). Using the data from (a), we show a correlation plot for R and $|I_3|$ from the same circuit.

a root function like

$$I_3 \sim C_0 \sqrt[p]{p * R}, \quad (19)$$

where C_0 is a constant, and power value x differs in specific QUBO problems. For the QUBO problems studied in our work, we find the value of x can be set to $x = 3$. As is depicted in Fig. 5, a range of value for C_0 and a peak of the C_0 distribution can be found in each cases, which reflects a positive proportional relation between I_3 and $\sqrt[p]{p * R}$ approximately. Additionally, the circuit may reach “entanglement barrier” when p is large [33, 34], then I_3 won’t increase with p . Therefore, this relation only holds for shallow QAOA circuits. When $p \gg 1$, both $I_3 \sim -2$ and $R \sim 1$, the ratio of I_3 and $\sqrt[p]{R}$ approximates to a constant.

To summarize, in this section we compare information scrambling in QAOA circuits with their corresponding success rates, which reflect the complexity of solving three different kinds of QUBO problems via QAOA. By comparing success rates R in the three cases, we find it is

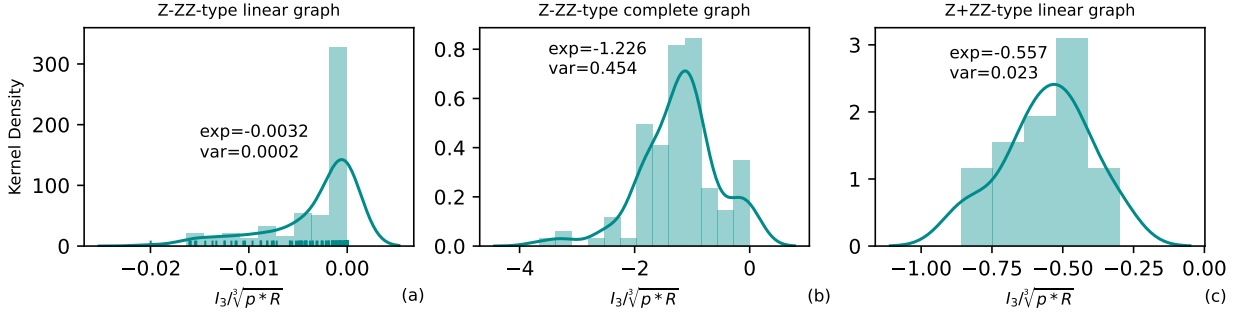


FIG. 5. Data distribution of $I_3/\sqrt[3]{p * R}$ for the three cases. Here in each cases we set $p \in [2, 15]$, and take 10^2 samplings for each p , to obtain success rate R when $\alpha \geq 0.996$ and average tripartite information I_3 .

sensitive to both factors of QUBO complexity \mathcal{C} , i.e. density of the graph D and weights of the graph $\{w_{ij}, h_k\}$. From those results, the positive correlation between tripartite information and complexity of the problems can be observed in the three kinds of graphs. Additionally, the fourth case, complete graph with $Z + ZZ$ -type Hamiltonians, should also be considered naturally. However, it's hard to find a non-degenerate solution, which cannot be mapped to a product ground state like above three cases. This could imply that for particular weights, it's difficult to avoid degeneracy in solutions, especially when the graph density is high.

B. Comparison between different edges of graphs

In this subsection, we explore a more direct way to characterize the complexity of problems. If we fix weights of the graphs, the complexity Eq. (1) has only one variable, density of the graphs D . Since in this work we only discuss $N = 7$, thus D can be expressed by the number of edges E according to Eq. (2). Then we can propose a relation between complexity and number of edges:

$$\mathcal{C} \propto E, \quad (20)$$

when $\{w_{ij}, h_k\}$ are fixed. To verify this correlation, next we focus on a set of graphs with fixed weights and different number of edges, whose corresponding Ising Hamiltonians are $Z - ZZ$ -type:

$$H_1 = + \sum_{i=1}^N Z_i - \sum_{i=1}^{N-1} Z_i Z_{i+1}, \quad (21a)$$

$$H_2 = + \sum_{i=1}^N Z_i - \sum_{i=1}^{N-1} Z_i Z_{i+1} - \sum_{i=1}^{N-2} Z_i Z_{i+2}, \quad (21b)$$

$$H_3 = + \sum_{i=1}^N Z_i - \sum_{i=1}^{N-1} Z_i Z_{i+1} - \sum_{i=1}^{N-2} Z_i Z_{i+2} - \sum_{i=1}^{N-3} Z_i Z_{i+3}, \quad (21c)$$

$$H_4 = + \sum_{i=1}^N Z_i - \sum_{i=1}^{N-1} Z_i Z_{i+1} - \sum_{i=1}^{N-2} Z_i Z_{i+2} - \sum_{i=1}^{N-3} Z_i Z_{i+3} - \sum_{i=1}^{N-4} Z_i Z_{i+4}, \quad (21d)$$

$$H_5 = + \sum_{i=1}^N Z_i - \sum_{i,j=1, i \neq j}^N Z_i Z_j. \quad (21e)$$

All the Hamiltonians in Eq. (21) have the ground state $|1\rangle^{\otimes N}$. The relation between number of edges of these graphs E , success rates R and tripartite information I_3 in QAOA circuit is depicted in Fig. 6.

From Fig. 6(a) we see, generally speaking, the success rates R is positively correlated with the number of edges E , which is in agreement with Eq. (20). However, as depth of the circuit goes deeper, the success rates seem stop increasing or even decrease, which is inconsistent with our ideal prediction.

We have mentioned the local minima problem for QAOA in Sec. III A. A deeper circuit depth means a more complex process of variational optimization, and one more layer takes a pair of new parameters. Therefore, the algorithm faces more local minima and most of them have low α values. Another interesting phenomenon in Fig. 6(a) is, as the success rates of computing $\langle H_1 \rangle_{min}$ to $\langle H_4 \rangle_{min}$ stops increasing, computing $\langle H_5 \rangle_{min}$ don't have to suffer from the problem. This may be explained that the complete graph is the most complex and needs more parameters for a good optimization, so when the layer p is larger, relatively it has more possibility to reach a high success rate.

From the distribution in Fig. 7 we can find the relation Eq. (19) holds for graphs in Eq. (21) as well. For a certain QUBO graph, one can estimate the value C_0 of Eq. (19) to obtain an equation between I_3 and the cube root success rate R . We can also observe the expectation value of C_0 from Fig. 7 increases as the number of edges E goes on. It is because the success rate R decreases when the QUBO problem becomes harder to solve.

Moreover, as the number of edges E can reflect complexity of QUBO problems directly in Eq. (20), we wonder if there is also a positive correlation between number of edges E and information scrambling I_3 . The tripartite information in QAOA circuits versus different E is depicted in Fig. 6(b), where we can observe a positive correlation between E and I_3 as well. Here, the Pearson correlation coefficients of E and I_3 are 0.8357, 0.8624, 0.8512 and 0.8761 for four different layers $p = 4, 6, 8, 10$.

IV. ENTANGLEMENT IN QAOA CIRCUIT VERSUS COMPLEXITY OF THE PROBLEMS

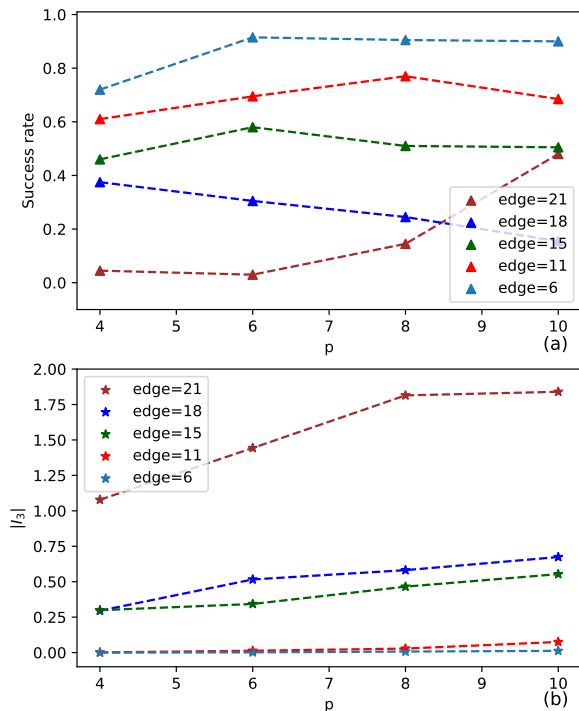


FIG. 6. The comparison between success rates for computing minimal mean values of Eq. (21) via p -layer QAOA and information scrambling in the circuit with number of qubits $N = 7$, in $Z-Z$ type Hamiltonians with different edges E and the same weights. (a). The success rates of QAOA of different layers when $\alpha \geq 0.996$ and 10^2 loops. (b). Average tripartite information of QAOA circuits corresponding to the success rates.

As we have discussed in previous sections, information scrambling is a global feature of a quantum channel. Next, we turn to more details for entanglement properties in the circuits. We still take Eq. (21) as the set of our interested QUBO problems with non-degenerate solutions, and their corresponding Ising Hamiltonians have the ground state $|1\rangle^{\otimes N}$. As have introduced in Sec. I, since both the initial and final state are separable, entanglement is only generated during the computing process. Therefore in this section, we explore how to quantify the

entanglement generated in a QAOA circuit, and its correlation with complexity of QUBO problems.

We first define a coarse-grained quantity for a QAOA circuit with a given layer p :

$$S_{max}^p = \max_{l \leq p, l \in \mathbb{Z}} \{ \bar{S}_l^p \}, \quad (22)$$

where \bar{S}_l^p has the form of Eq. (10), which is the average one-qubit entanglement entropy of every layer $l \leq p$ in the p -layer circuit. Eq. (22) means the maximum of average one-qubit entanglement entropy among all \bar{S}_l^p . After that, we present the maximal entanglement entropy generated in the circuits during the process of computing minimal mean values of Hamiltonians of Eq. (21) in Fig. 8. From this figure, we can see the tendency that the more number of edges E the graph has, the more entanglement is generated in the circuit. Similar to Sec. III, we quantify the correlation via Pearson coefficients with number of edges E and maximal one-qubit entanglement entropy S_{max}^p , they are 0.8982, 0.9446, 0.9033, 0.9255 for layers $p = 4, 6, 8, 10$ respectively.

To this point, a question raises naturally: What about the entanglement properties inside one layer? As previous studies of entanglement in QAOA circuit only take one “layer” as a unit, what happens inside one layer has not been investigated yet. According to the layer of QAOA circuit shown in Fig. 1, the two-qubit gates represent the terms $e^{-i\gamma_i Z_j Z_k}$ in Eq. (4), all of them can generate entanglement. Therefore, in the following we step into each layer and focus on total entanglement accumulated in QAOA circuits.

We now introduce a proper characterization of entanglement accumulation in p -layer QAOA circuit in the form of

$$\mathcal{A} = \text{Area}(\bar{S} * p), \quad (23)$$

which is the area of $\bar{S} - p$ plot for average one-qubit entanglement entropy \bar{S} generated during the evolution of p -layer QAOA circuit. Ideally, we expect the accumulation \mathcal{A} is always positively correlated with number of edges E . However, due to the randomness of initial parameters $\{\vec{\beta}_0, \vec{\gamma}_0\}$, entanglement accumulation of the same layer in the same computing process can be very different from each other. For example, two different typical structures of entanglement accumulation in the process of computing $\langle H_5 \rangle_{min}$ when $p = 6$ is shown in Fig. 10. The structure in Fig. 10(a) only demands large entanglement at first two layers, whereas entanglement in Fig. 10(b) is always large until the final step. Thus, to obtain a practical quantity describing entanglement accumulation, we still need a number of samplings and consider average values.

Here, we present the distribution of \mathcal{A} for 50 samplings per layer and per problem in Fig. 12. We can find for harder problems, the “tails” of probability density become larger, which means the proportion of entanglement structures like Fig. 10(b) increases, and indicates a

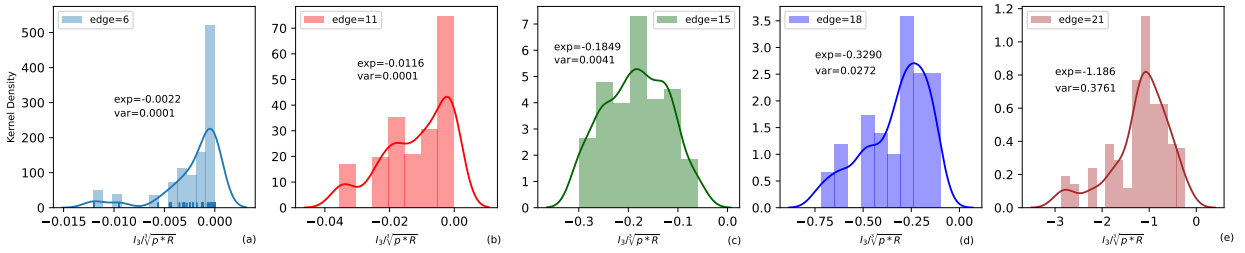


FIG. 7. Data distribution of $I_3/\sqrt[3]{p} * R$ for the QUBO problems in Eq. (21). Here in each cases we set $p = 4, 6, 8, 10$, and take 10^2 samplings for each p , to obtain success rate R when $\alpha \geq 0.996$ and average tripartite information I_3 .

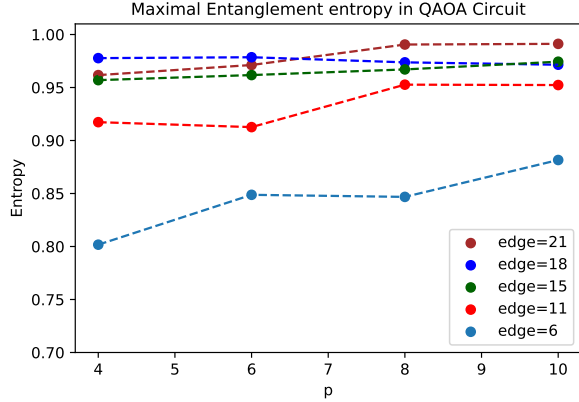


FIG. 8. One-qubit maximal entanglement entropy in p -layer QAOA circuits during the process of computing minimal mean values of Ising Hamiltonians in Eq. (21). Here we choose four different layers: $p = 4, 6, 8, 10$, and take an average of 10^2 data.

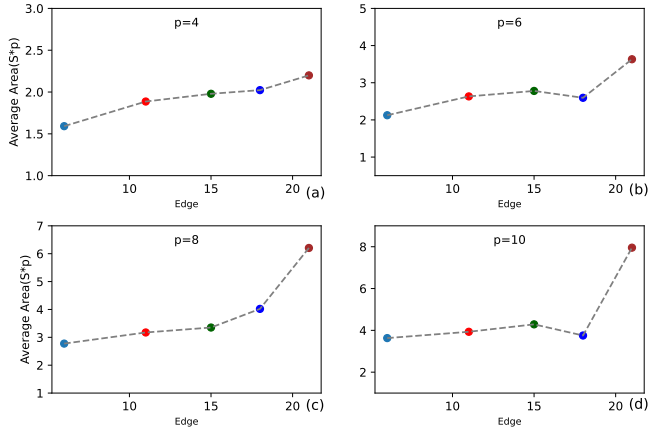


FIG. 9. Average entanglement accumulation \bar{A} to reach $\alpha \geq 0.996$ during the process of computing minimal mean values of Hamiltonians in Eq. (21) with four fixed layers $p = 4, 6, 8, 10$. We take an average of 50 samplings for each case.

requirement for more entanglement accumulation. Moreover, by taking average values of these samplings, we obtain a positive correlation between average areas of entanglement accumulation \bar{A} and number of edges E of the graphs of Eq. (21), which is shown in Fig. 9.

However, as the layer p increases, the effect of “en-

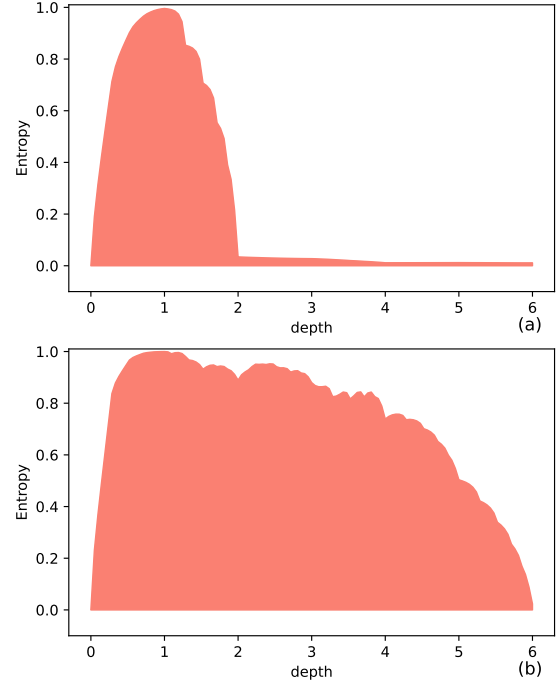


FIG. 10. Two examples of $S - p$ plots for entanglement entropy accumulation when $p = 6$, edges of $ZZ = 21$. Here we calculate \bar{S} after each two-qubit gate in the circuit, and the caption “depth” means the layers $l \leq p$ of one p -layer QAOA circuit.

entanglement barrier” cannot be neglected [33, 34], which can weaken the strength of positive correlation. For the correlation coefficients between average areas of entanglement accumulation \bar{A} and number of edges E , we can observe this decrease. As is shown in Fig. 11, from which we find that when $p \gg 20$, it can be harder to observe the positive correlation because the entanglement barrier arrives.

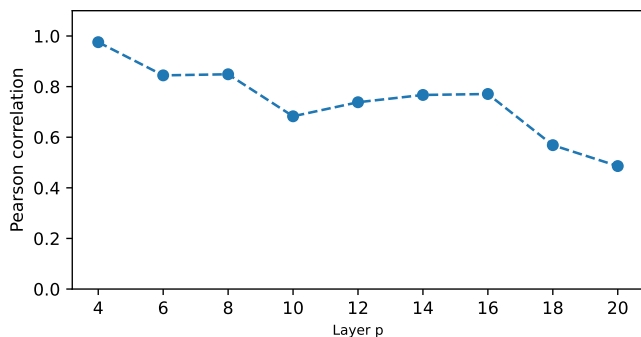


FIG. 11. The decrease of Pearson correlation coefficients between average entanglement accumulation $\bar{\mathcal{A}}$ and number of graph edges E as the layer p goes on.

V. CONCLUSIONS AND OUTLOOK

In this work, we have addressed the question of how much quantum resource is consumed for solving QUBO problems with different complexity in QAOA circuits. More precisely, we characterize quantum resource in QAOA circuits by two concepts in quantum information, information scrambling and entanglement, and characterize complexity of problems by success rates and number of edges of graphs. By taking QAOA circuits as unitary quantum channels, we use tripartite mutual information to quantify information scrambling. Next, we use the maximal entanglement entropy among every layers in QAOA circuits to present how much entanglement is needed in the whole computing process. After that, we study entanglement accumulation caused by two-qubit gates inside every layers in QAOA circuits, where we define an effective quantity to describe this process, namely an average area of entanglement entropy generated in the circuits and depth of the circuits.

Our main contribution is to present a positive correlation between complexity of QUBO problems and quantum resources including information scrambling and entanglement in QAOA circuits. Specially, we find the tripartite mutual information in QAOA circuits is positively proportional to the cube root of success rate approximately. Apart from this contribution, we clarify the factors related to the complexity of QUBO problems \mathcal{C} : graph weights $\{w_{ij}, h_k\}$ and graph density D . Then, we use success rate R to quantify the complexity in specific cases of our work. After that, we offer two quantities to describe how much entanglement, i.e. the maximal entanglement entropy Eq. (22) and the area of entanglement accumulation Eq. (23), is required in QAOA circuits, which can be useful for further applications to practical quantum circuits.

To give a deeper explanation to the positive correlation, it is noteworthy that our results uncover a map between computational complexity of QUBO models, and physical complexity of the unitary channels in corresponding QAOA circuits. More precisely, the compu-

tational complexity of a QUBO model is governed by its geometric structure, which is a mathematical property. This geometric structure, in turn, dictates the physical structure of the corresponding Ising Hamiltonian. Ultimately, this physical structure determines complexity of the circuit employed in QAOA. From the perspective of many-body physics, for an Ising Hamiltonian exhibiting increased complexity in its physical structure, achieving evolution to its ground state from the initial state of QAOA becomes significantly more complex. Therefore, the process requires more quantum resource. In this work, we numerically present the map between the two complexities in our results. For future works, we will explore the connections more analytically.

Moreover, several remarks and outlooks including scrambling and entanglement are discussed as follows.

In the part of information scrambling, as we have discussed in Sec. III, the circuits are more scrambled when the problem is more complex. However, there is a question: How to compare the complexity of case Eq. (16) and case Eq. (17)? Obviously the success rates of Eq. (17) is much lower, but its tripartite information is smaller than that of Eq. (16). To this extent, we need further studies to well-define the relation between complexity \mathcal{C} in a general context.

It should be pointed out that the resource of information scrambling includes two aspects: entanglement scrambling and magic scrambling [8, 23]. Among these aspects, magic is said to be a complete quantum resource as it cannot be simulated by classical computers, and it is used to quantify complexity of fidelity estimation [43, 44]. Therefore, an interesting future work is to characterize how much magic generated in QAOA circuits, which can be an important direction for demonstrating quantum advantages beyond classical computation.

In the part of entanglement, the average area of entanglement accumulation $\bar{\mathcal{A}}$ can be viewed as an overall entanglement resource required in the process of solving target problems, which can be a general quantity not only for a certain kind of problems like Eq. (21). We can apply this quantity to all QUBO problems with non-degenerate solutions, and generalizing the quantity to include problems with degenerate solutions is also a promising topic to be discussed in the future. Moreover, as is shown in Fig. 10 and Fig. 12, $\bar{\mathcal{A}}$ for the same problem can be very different due to random choices of $\{\beta_0, \gamma_0\}$. It is interesting to consider the entanglement accumulation as a special feature of QAOA optimization process. Then, we can improve the algorithm by selecting the output that requires the least amount of entanglement accumulation among outputs with the same α value.

In summary, our results try to build a connection between the computational complexity of mathematical problems and physical quantum resources required for solving them in corresponding QAOA circuits. It should be noticed that our discussion is so far limited to small number of qubits and easy problems. In further studies, a generalization of our results may have a wide applica-

tion in areas of not only quantum computation but also many-body physics, such as many-body localization [45], quantum phase transitions [46], and so on.

ACKNOWLEDGMENTS

We thank Ya-Nan Pu, Yunheng Ma and Yanwu Gu for useful discussions. This work is supported by Beijing Natural Science Foundation (No.Z220002).

DATA AVAILABILITY STATEMENT

This manuscript has associated data generated from quantum software *Qcover* developed by Beijing Academy of Quantum Information Sciences, with the GitHub link: <https://github.com/BAQIS-Quantum/Qcover/tree/main/Qcover/research>. [Authors' comment: The datasets generated for the study, together with the code used for the analysis, are available from the corresponding author on request.]

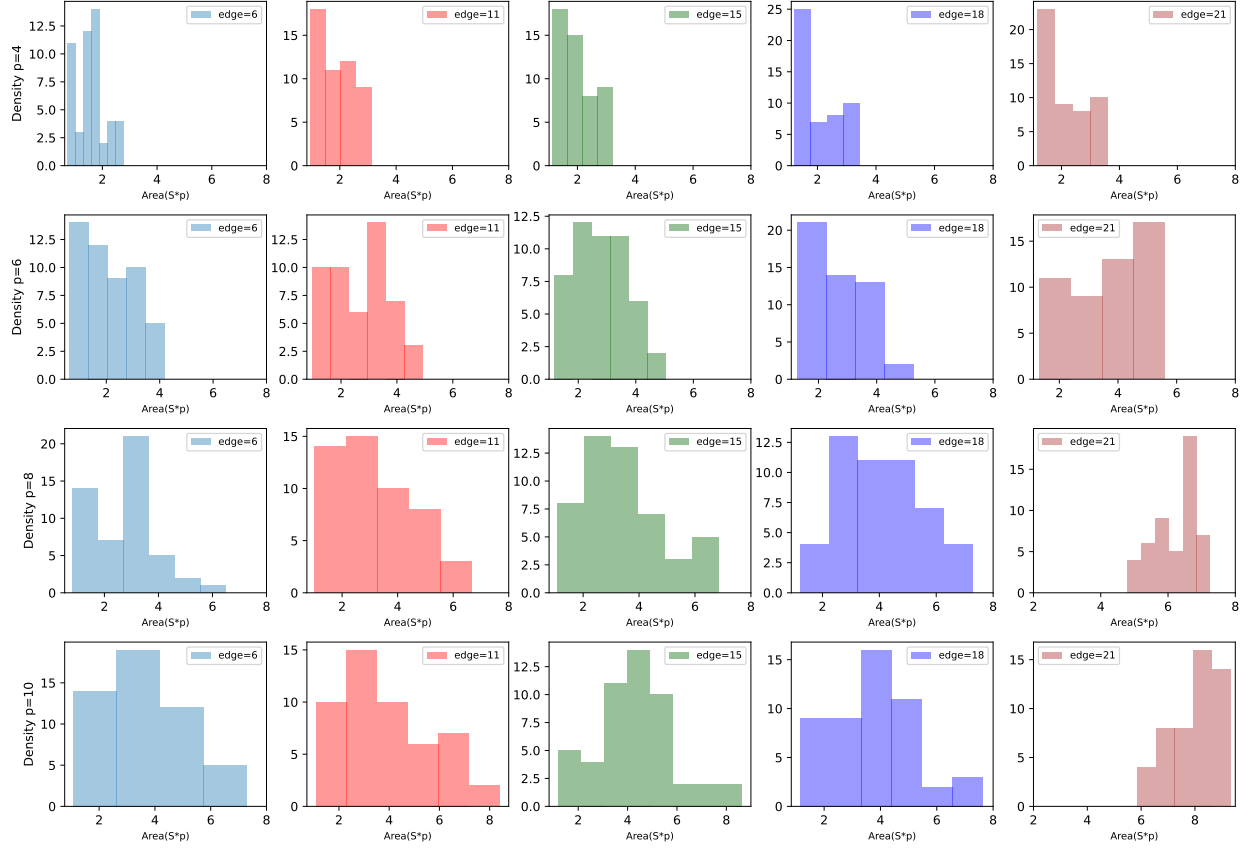


FIG. 12. The distributions and probability density of areas of $S - p$ plots with different QAOA layers and problems for 50 samplings. Figures from up to down are distributions of the same problems for layers $p = 4, 6, 8, 10$. Figures from left to right are distributions of the same layers for the problems $\langle H_1 \rangle_{min}$ to $\langle H_5 \rangle_{min}$.

-
- [1] E. Chitambar and G. Gour, Quantum resource theories, *Rev. Mod. Phys.* **91**, 025001 (2019).
- [2] R. Horodecki, P. Horodecki, M. Horodecki, and K. Horodecki, Quantum entanglement, *Rev. Mod. Phys.* **81**, 865 (2007).
- [3] J. Preskill, Quantum computing in the nisq era and beyond, *Quantum* **2**, 79 (2018).
- [4] P. Hosur, X.-L. Qi, D. A. Roberts, and B. Yoshida, Chaos in quantum channels, *J. High Ener. Phys.* **2016**, 4 (2022).
- [5] K. A. Landsman, C. Figgatt, T. Schuster, N. M. Linke, B. Yoshida, N. Y. Yao, and C. Monroe, Verified quantum information scrambling, *Nature* **567**, 61–65 (2019).
- [6] S. Xu and B. Swingle, Scrambling dynamics and out-of-time ordered correlators in quantum many-body systems: a tutorial, arXiv:2202.07060 (2022).
- [7] A. Ahmadi and E. Greplova, Quantifying quantum computational complexity via information scrambling, arXiv:2204.11236 (2022).
- [8] R. J. Garcia, K. Bu, and A. Jaffe, Resource theory of quantum scrambling, *Proc. Natl. Acad. Sci. U.S.A.* **120**, 2217031120 (2023).
- [9] P. Hayden and J. Preskill, Black holes as mirrors: quantum information in random subsystems, *J. High Ener. Phys.* **2007**, 120 (2007).
- [10] D. Harlow, Jerusalem lectures on black holes and quantum information, *Rev. Mod. Phys.* **88**, 015002 (2016).
- [11] B. Yoshida, Firewalls vs. scrambling, *J. High Ener. Phys.* **2019**, 132 (2019).
- [12] S. F. Oliviero, L. Leone, S. Lloyd, and A. Hamma, Unscrambling quantum information with clifford decoders, arXiv:2212.11337 (2022).
- [13] L. Leone, S. F. Oliviero, S. Lloyd, and A. Hamma, Learning efficient decoders for quasi-chaotic quantum scramblers, arXiv:2212.11338 (2022).
- [14] J. Harris, B. Yan, and N. A. Sinitsyn, Benchmarking information scrambling, *Phys. Rev. Lett.* **129**, 050602 (2022).
- [15] B. Yan and N. A. Sinitsyn, Recovery of damaged information and the out-of-time-ordered correlators, *Phys. Rev. Lett.* **125**, 040605 (2020).
- [16] H. Shen, P. Zhang, Y.-Z. You, and H. Zhai, Information scrambling in quantum neural networks, *Phys. Rev. Lett.* **124**, 200504 (2020).
- [17] Y. Wu, P. Zhang, and H. Zhai, Scrambling ability of quantum neural network architectures, *Phys. Rev. Research* **3**, L032057 (2021).
- [18] R. J. Garcia, K. Bu, and A. Jaffe, Quantifying scrambling in quantum neural networks, *J. High Ener. Phys.* **2022**, 27 (2022).
- [19] J. Cotler, N. Hunter-Jones, J. Liub, and B. Yoshida, Chaos, complexity, and random matrices, *J. High Ener. Phys.* **2017**, 48 (2017).
- [20] D. A. Roberts and B. Yoshida, Chaos and complexity by design, *J. High Ener. Phys.* **2017**, 121 (2017).
- [21] A. Bhattacharyya, L. K. Joshib, and B. Sundar, Quantum information scrambling: from holography to quantum simulators, *Eur. Phys. J. C* **82**, 458 (2022).
- [22] E. Iyoda and T. Sagawa, Scrambling of quantum information in quantum many-body systems, *Phys. Rev. A* **97**, 042330 (2018).
- [23] X. Mi and et al., Information scrambling in quantum circuits, *Science* **374**, 1479 (2021).
- [24] Q. Zhu and et al., Observation of thermalization and information scrambling in a superconducting quantum processor, *Phys. Rev. Lett.* **128**, 160502 (2022).
- [25] A. Kandala, A. Mezzacapo, K. Temme, M. Takita, M. Brink, J. M. Chow, and J. M. Gambetta, Hardware-efficient variational quantum eigensolver for small molecules and quantum magnets, *Nature* **549**, 242–246 (2017).
- [26] J. Biamonte, P. Wittek, N. Pancotti, P. Rebentrost, N. Wiebe, and S. Lloyd, Quantum machine learning, *Nature* **549**, 195–202 (2017).
- [27] E. Farhi and J. Goldstone, A quantum approximate optimization algorithm, arXiv:1411.4028 (2014).
- [28] A. P. Punnen, *The Quadratic Unconstrained Binary Optimization Problem* (Springer Nature, 2022).
- [29] J. Wu and T. H. Hsieh, Variational thermal quantum simulation via thermofield double states, *Phys. Rev. Lett.* **123**, 220502 (2019).
- [30] D. Fitzek, T. Ghandriz, L. Laine, M. Granath, and A. F. Kockum, Applying quantum approximate optimization to the heterogeneous vehicle routing problem, arXiv:2110.06799 (2021).
- [31] R. Wiersema, C. Zhou, Y. Sereville, J. F. Carrasquilla, Y. B. Kim, and H. Yuen, Exploring entanglement and optimization within the hamiltonian variational ansatz, *Phys. Rev. X Quantum* **1**, 020319 (2020).
- [32] P. Díez-Valle, D. Porras, and J. J. García-Ripoll, Quantum variational optimization: The role of entanglement and problem hardness, *Phys. Rev. A* **104**, 062426 (2021).
- [33] Y. Chen, L. Zhu, C. Liu, N. J. Mayhall, E. Barnes, and S. E. Economou, How much entanglement do quantum optimization algorithms require?, arXiv:2205.12283 (2022).
- [34] M. Dupont, N. Didier, M. J. Hodson, J. E. Moore, and M. J. Reagor, Entanglement perspective on the quantum approximate optimization algorithm, *Phys. Rev. A* **106**, 022423 (2022).
- [35] R. Sreedhar, P. Vikstål, M. Svensson, A. Ask, G. Johansson, and L. García-Álvarez, The quantum approximate optimization algorithm performance with low entanglement and high circuit depth, arXiv:2207.03404 (2022).
- [36] A. Kitaev and J. Preskill, Topological entanglement entropy, *Phys. Rev. Lett.* **96**, 110404 (2006).
- [37] W.-F. Zhuang, Y.-N. Pu, H.-Z. Xu, X. Chai, Y. Gu, Y. Ma, S. Qamar, C. Qian, P. Qian, X. Xiao, and D. E. L. M.-J. Hu, Efficient classical computation of quantum mean values for shallow qaoa circuits, arXiv:2112.11151 (2021).
- [38] L. Zhou, S.-T. Wang, S. Choi, H. Pichler, and M. D. Lukin, Quantum approximate optimization algorithm: Performance, mechanism, and implementation on near-

- term devices, *Phys. Rev. X* **10**, 021067 (2020).
- [39] B. Zhang, A. Sone, and Q. Zhuang, Quantum computational phase transition in combinatorial problems, *npj Quantum Information* **8**, 87 (2022).
- [40] J. Håstad, Some optimal inapproximability results, *Journal of the ACM* **48**, 4 (2001).
- [41] S. Sakai, M. Togasaki, and K. Yamazaki, A note on greedy algorithms for the maximum weighted independent set problem, *Discrete Applied Mathematics* **126**, 313 (2003).
- [42] L. Bittel and M. Kliesch, Training variational quantum algorithms is np-hard, *Phys. Rev. Lett.* **127**, 120502 (2021).
- [43] L. Leone, S. F. Oliviero, and A. Hamma, Nonstabilizer-ness determining the hardness of direct fidelity estimation, *Phys. Rev. A* **107**, 022429 (2023).
- [44] L. Leone, S. F. Oliviero, and A. Hamma, Learning t-doped stabilizer states, arXiv:2305.15398 (2023).
- [45] D. A. Abanin, E. Altman, I. Bloch, and M. Serbyn, Colloquium: Many-body localization, thermalization, and entanglement, *Rev. Mod. Phys.* **91**, 021001 (2019).
- [46] J. Dziarmaga, Dynamics of a quantum phase transition and relaxation to a steady state, *Adv. in Phys.* **59**, 1063 (2010).